chemosensors

MDPI

Article

Sensitive Detection of Aflatoxin B1 in Foods Using Aptasensing Based on FGO-Mediated CdTe QDs

Puye Liang, Sihan Liu, Qinqing Han, Kaixuan Zhou, Tiange Li, Xianqing Huang, Lianjun Song * and Tianlin Wang *

College of Food Science and Technology, Henan Agricultural University, Zhengzhou 450002, China; liangpuye@stu.henau.edu.cn (P.L.); liusihan@stu.henau.edu.cn (S.L.); hanqinqing@stu.henau.edu.cn (Q.H.); zhoukaixuan@stu.henau.edu.cn (K.Z.); litiange@henau.edu.cn (T.L.); hxq8210@126.com (X.H.)
* Correspondence: slj69@126.com (L.S.); wangtianlin@henau.edu.cn (T.W.)

Abstract: Aflatoxin B_1 (AFB_1) exhibits high toxicity and has the potential to induce cancer, deformities, and mutations. It is therefore highly desirable that sensitive and straightforward methods for detecting AFB_1 be developed. In this study, due to the high specific adsorption capacity of AFB_1 aptamers, we applied a sensing strategy based on quantum dots (QDs) and carboxyl-functionalized graphene oxide (FGO) to construct a simple fluorescence quenching platform. FGO and CdTe QDs modified with AFB_1 aptamers cause a FRET effect that produces CdTe QDs with yellow-green fluorescence quenching. When AFB_1 is present, aptamers form complexes with it and CdTe QDs leave the quenching platform, resulting in fluorescence recovery. In this study, we used a fluorescence aptasensor with a wide detection range of 0.05 to 150 ng/mL and a low limit of detection (LOD) of 8.2 pg/mL. The average recoveries of AFB_1 in peanut and pure milk samples ranged from 94.5% to 107.0%. The aptasensor also exhibited the advantages of simple operation, low cost, and good stability. The sensing strategy reported here can thus serve as a potential candidate for the rapid detection of AFB_1.

Keywords: aflatoxin B_1; aptasensor; carboxyl-functionalized graphene oxide; CdTe QDs; FRET

check for updates

Received: 4 March 2025
Revised: 1 April 2025
Accepted: 9 April 2025
Published: 11 April 2025

Citation: Liang, P.; Liu, S.; Han, Q.; Zhou, K.; Li, T.; Huang, X.; Song, L.; Wang, T. Sensitive Detection of Aflatoxin B1 in Foods Using Aptasensing Based on FGO-Mediated CdTe QDs. *Chemosensors* **2025**, *13*, 141. https://doi.org/10.3390/chemosensors13040141

Copyright: © 2025 by the authors. Licensee MDPI, Basel, Switzerland. This article is an open access article distributed under the terms and conditions of the Creative Commons Attribution (CC BY) license (https://creativecommons.org/licenses/by/4.0/).

1. Introduction

Aflatoxin B_1 (AFB_1) is a type of harmful substance generated by *Aspergillus flavus* and *Aspergillus parasiticus*. It is easy for agricultural products to be contaminated by AFB_1 [1,2], which has been closely associated with immunosuppression, kidney disease, and even cancer [3–6]; indeed, AFB_1 is recognized by the International Organization for Cancer as a Class I carcinogen. Contamination of food by AFB_1 is now a major global issue, and the development of effective and user-friendly AFB_1 detection strategies is now highly anticipated.

Today, HPLC, TLC, and LC-MS are the most widely used conventional AFB_1 detection methods [7–9]. These approaches have advantages in terms of detection sensitivity and accuracy. However, their application in rapid detection is constrained by several limitations; these include cumbersome measurement procedures, high costs, and the unsuitability of such methods for screening large samples. In recent years, immunological methods have been developed for the simple and rapid detection of AFB_1, primarily including electrochemical immunoassay, ELISA, and antigen microarray [10–12]. However, the high cost of antibodies used in immunological methods is a concern that cannot be overlooked. Compared with antibodies, aptamers are easier and cheaper to produce [13]. Consequently,

aptamers are now widely used as excellent candidates for the detection of AFB_1. Yao et al. employed a high-efficiency magnetic chain graphene oxide-based SELEX to generate circular aptamers that bind AFB_1 with high affinity and selectivity [14]. Sun et al. reported an AFB_1 detection method based on a real-time quantitative polymerase chain reaction (PCR) with a detection limit of 0.03 pg/mL [15]. Undoubtedly, this technology delivers ultra-high sensitivity, yet its potential is greatly hindered by the requirement for sophisticated real-time PCR instruments and various complex PCR reagents. There is, therefore, an urgent need for the development of aptamer-based strategies that enable the simple and rapid monitoring of AFB_1 in foods.

With continuous progress in nanotechnology, fluorescent nanomaterials are now widely applied in sectors such as biosensing, bioimaging, and drug delivery, owing to their small size, their high specific surface areas, and their versatile functional characteristics [16–20]. In addition, some recognition elements such as aptamers can be easily modified on the surfaces of nanomaterials, enabling the construction of fluorescent probes that specifically recognize target molecules [21]. Fluorescent quantum dots (QDs), as a typical representative of fluorescent nanomaterials, possess a range of remarkable advantages, including narrow and symmetrical fluorescence emission peaks, large Stokes shifts, excellent photostability, and good water solubility. QDs therefore play an important role in rapid visual detection [22–24]. In addition, graphene oxide (GO) is known as a quenching agent with broad-spectrum absorption. GO delivers excellent fluorescence quenching performance in detection fields, assisted by the fluorescence resonance energy transfer (FRET) effect [25,26]. GO is therefore well suited for use in the construction of an aptamer-based fluorescence response system.

In this study, we sought to construct an aptasensor with enhanced biocompatibility, tailored to suit the intricate detection environments found in food. A GO surface was modified with carboxyl functional groups (FGO) to increase its water solubility. In addition, an aptasensor was prepared for the detection of AFB_1 based on FRET between FGO and CdTe QDs modified with the AFB_1 aptamer. An aptamer with specificity for AFB_1 was first coupled with yellow-green CdTe QDs. Upon exposure to AFB_1, the fluorescence of CdTe QDs was quenched because of the interaction of the aptamer with FGO. After the recognition of the AFB_1, the strong binding between AFB_1 and its aptamer increased the distance between the quantum dots and FGO, thereby blocking the FRET effect. Finally, the fluorescence intensity of CdTe QDs was found to be positively correlated with AFB_1 concentrations.

2. Materials and Methods

2.1. Reagents

Aptamer (5′–NH_2–$(CH_2)_6$–CACGTGTTGTCTCTCTCTGTGTCTCGTG–3′) was synthesized by Shanghai Shenggong Biotechnology Co., Ltd. AFB_1, aflatoxin M1 (AFM_1), fumonisin B1 (FB_1), zearalenone (ZEN), patamycin (PAT), and deoxynivalenol (DON) were purchased from Aladdin Co. Ltd. (Shanghai, China). All other chemicals used in the study were analytical grade. Aqueous solutions were obtained from ultrapure water (18.2 MΩ·cm).

2.2. Instruments

Raman spectra were obtained using a DXR2xi Raman imaging microscope system (Thermo, Waltham, MA, USA). Fourier-transform infrared (FTIR) spectra were recorded on a TENSOR 27 FT-IR spectrometer (Bruker, Karlsruher, Germany). Morphology was observed using a JEM-2100 Pro transmission electron microscope (JEOL, Amagasaki, Japan). Fluorescence spectra were recorded using a LUMINA fluorescence spectrometer (Thermo,

Waltham, MA, USA). UV absorption spectra were measured using a UV-2600 spectrophotometer (Shimadzu, Tokyo, Japan).

2.3. Experimental Procedures

2.3.1. Preparation of GO and FGO

GO and FGO were prepared according to our previous study [27]. A 2 g amount of graphite powder and a 2 g amount of $NaNO_3$ were dissolved in 80 mL of H_2SO_4 (98%) and stirred vigorously at 1500 rpm for 20 min to obtain a uniform dispersion in an ice bath. Next, 12 g of $KMnO_4$ was slowly added to the mixture. The mixture was then continuously stirred at 40 °C for 2 h to obtain a dark green solution. Next, 80 mL of deionized water was added. The mixture was then heated up to 90 °C and stirred for another 1 h. The unreacted $KMnO_4$ was removed using H_2O_2 (30%). By repeating the centrifugation and filtration process, the sediment was washed with HCl (5%) and deionized water several times, then dried at 60 °C for 24 h to obtain GO. To obtain FGO, GO was dispersed in deionized water until a final concentration of 1 mg/mL was obtained. Then, 1.5 g of NaOH and 1 g of chloroacetic acid were added to the GO solution and continuously stirred for 2 h. After centrifugation, the FGO was obtained after drying at 60 °C for 24 h.

2.3.2. Preparation of CdTe QDs

On the basis of previous research, with some minor modifications [28], 2 g of trisodium citrate, 0.5 g of cadmium chloride ($CdCl_2$), 0.5 g of mercaptosuccinic acid, 0.35 g of sodium tellurite (Na_2TeO_3), and 0.1 g of sodium borohydride ($NaBH_4$) were dispersed in 100 mL of deionized water. After stirring for 30 min, the mixture was transferred to a stainless-steel autoclave and heated at 160 °C for 6 h. The cooled solution was centrifuged at 12,000 rpm for 15 min and filtered using a 0.22 μm filter. Finally, the CdTe QDs were obtained after freeze-drying under vacuum.

2.3.3. Ligation of CdTe QDs with AFB_1 Aptamer

A 5 mL amount of 1.0 mg/mL CdTe QDs solution was added to the mixture containing EDC (5 mL, 0.02 M) and NHS (5 mL, 0.2 M) and treated with ultrasound for 2 h. Then, 5 mL of 1.6 μM AFB_1 aptamer was added to the above mixed solution and incubated at 4 °C for 24 h. The CdTe-Apt QDs were collected after centrifugation at 12,000 rpm for 15 min. The CdTe-Apt QDs were suspended in phosphate-buffer solution (0.01 M, pH 7.4) for AFB_1 detection.

2.4. CdTe-Apt/FGO Aptasensing System for Detection of AFB_1

FGO and CdTe-Apt QDs were added to phosphate-buffer solution (PBS, 0.01 M, pH 7.4) until the final concentrations were 0.1 mg/mL and 0.6 mg/mL, respectively. The CdTe-Apt/FGO aptasensing system was obtained after shaking for 2 min. Next, AFB1 standards of different concentrations (0.02 ng/mL, 0.05 ng/mL, 0.1 ng/mL, 0.5 ng/mL, 1 ng/mL, 5 ng/mL, 10 ng/mL, 50 ng/mL, 100 ng/Ml, 150 ng/mL, 200 ng/mL, and 250 ng/mL) were added to the aptasensing system. The fluorescence spectra were recorded to evaluate the fluorescence recovery ability of the developed aptasensor in the presence of AFB_1.

2.5. Specificity and Anti-Interference Ability

The prepared aptasensor was used to detect the samples with interference toxins (FB1, ZEN, DON, and PAT) and AFB_1. The concentrations of interference toxins were 5 times higher than the concentration of AFB_1. Changes in the fluorescence signal response caused by AFB_1 and interference toxins were studied to evaluate the anti-interference ability.

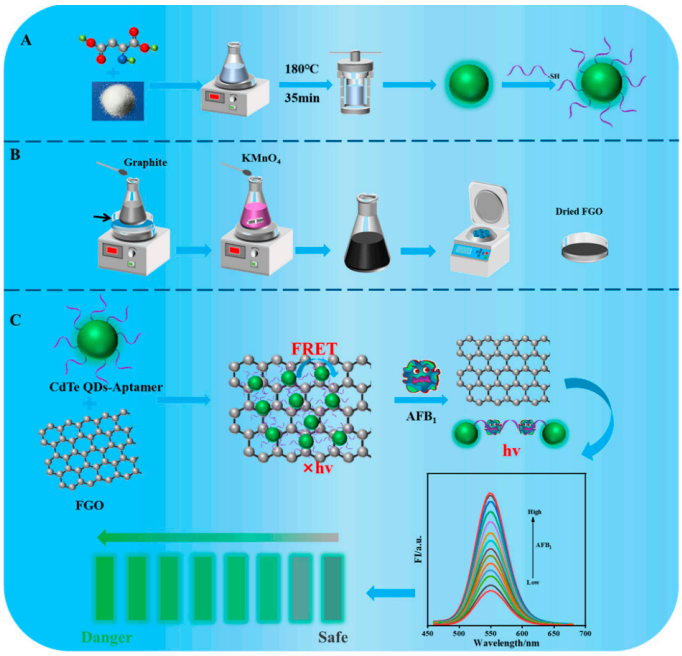
2.6. Detection of AFB_1 in Real Samples

Pure milk and peanut powder were purchased from a local supermarket for use as actual samples. A 2 mL amount of pure milk and a 1 g amount of peanut powder were each dispersed in 50 mL of methanol–water (7:3, *v*/*v*). After 10 min of ultrasound treatment, the standard AFB_1 solution (0 ng/mL, 0.1 ng/mL, 1.0 ng/mL, and 10 ng/mL) was added to the samples and continuously stirred for 30 min. The supernatant was first collected after centrifugation at 12,000 rpm for 15 min and then filtered using a 0.22 μm organic filter membrane. The treated samples were then subjected to evaluation by the aptasensor and HPLC.

3. Results

3.1. Construction of CdTe-Apt/FGO Fluorescent Aptasensor

CdTe QDs were obtained using a one-pot hydrothermal method (Scheme 1A). The synthesis processes used for GO and FGO were based on graphene as a precursor and $KMnO_4$ as an oxidant (Scheme 1B). The principle of an aptasensing system based on CdTe-Apt/FGO is that CdTe QDs fluorescence quenching is caused by strong absorption through noncovalent π-π stacking interaction at the interface between the aptamer modified on CdTe QDs and the FGO layer [29] (Scheme 1C). Because complexes of CdTe-Apt/FGO are in a ground state, CdTe QDs may achieve fluorescence quenching mainly through FRET [30,31]. We found that, upon exposure to AFB_1, a stronger combination occurred between AFB_1 and its aptamer, weakening the interaction between the aptamer and FGO and hindering the FRET effect. The fluorescence of CdTe QDs was restored as the AFB_1 concentration increased. The aptasensor demonstrated significant advantages in terms of speed, sensitivity, and selectivity. Moreover, it provided a new theoretical reference for the visualization and rapid detection of AFB_1 in actual samples.



Scheme 1. The synthesis process of CdTe-Apt (**A**) and (**B**). Preparation of CdTe-Apt/FGO aptasensor and its detection principle for AFB_1 (**C**).

3.2. Characterization of FGO and CdTe QDs

Raman spectrum analysis clearly determined the proportion of graphite carbon in FGO. The Raman spectra of GO and FGO were both measured (Figure 1A). The vibration of

graphite carbon induced a characteristic peak in the G band at around ~1596 cm^{-1}, while the vibration of disordered/oxidized carbon caused a distinct characteristic peak in the D band at around ~1355 cm^{-1} [32,33]. The I_D/I_G ratios of GO and FGO were obtained using G/D-band calculation. A higher I_D/I_G value in FGO indicated that carboxylation increased the carbon content of sidewall defects or edges. In the FT-IR spectra of GO (Figure 1B), hydroxyl stretching caused a strong peak at around 3429 cm^{-1}. The asymmetric and symmetric stretching vibrations of C–H bonds caused two characteristic peaks to appear at 2920 and 2850 cm^{-1}. The peaks at 1622 cm^{-1}, 1373 cm^{-1}, and 992 cm^{-1} were attributed to the stretching vibrations of the C=O band, the C–OH and C–O bonds, and the C–O bond, respectively. In addition, the peak at 1728 cm^{-1} belonged to the C=C bond of the Sp^2 hybrid [34]. The FT-IR spectrum of FGO revealed that, in addition to containing functional groups similar to those of GO, it was also functionalized with oxygen-containing groups. As illustrated in Figure 1C, FGO displayed a distinct two-dimensional sheet-like structure. Its larger specific surface area facilitated the better adsorption of small molecules [35]. UV absorption spectra are displayed in Figure 1D. Based on the $\pi \rightarrow \pi^*$ conjugated transition effect of aromatic C=C bonds, an absorption peak at around 227 nm belonged to GO. However, due to the abundant carboxyl functional groups in FGO, its peak position redshifted to 264 nm. Additionally, FGO displayed a broad absorption band from 200 nm to 800 nm, demonstrating its excellent quenching ability.

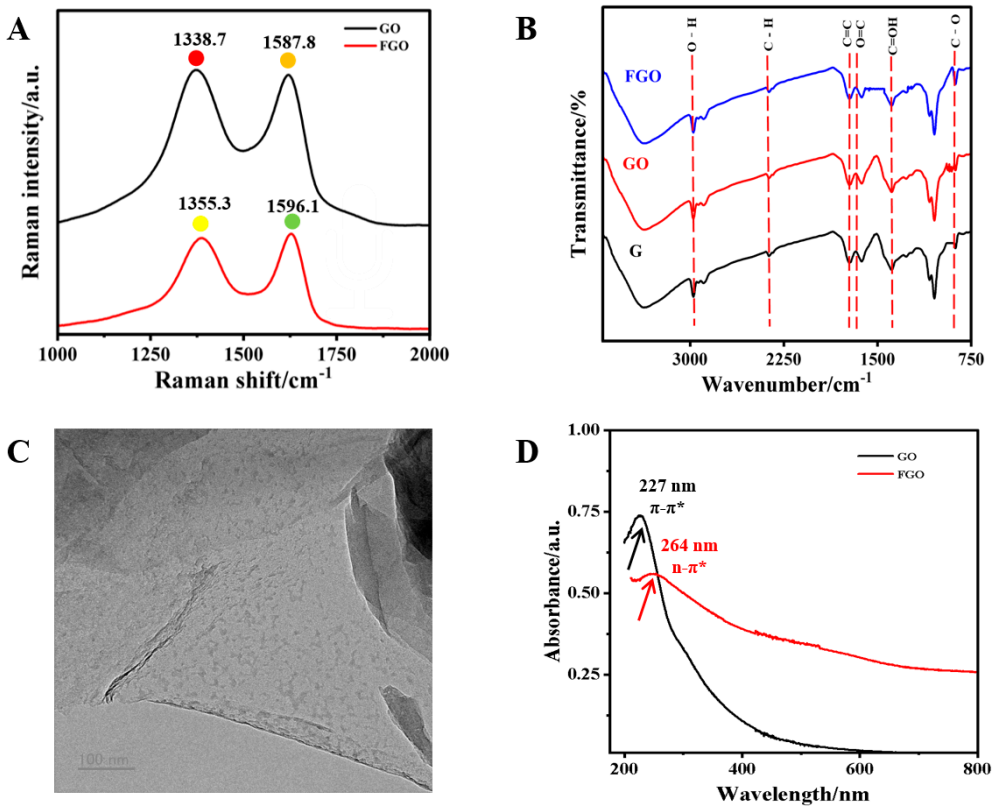


Figure 1. (**A**) Raman of GO and FGO; (**B**) FTIR spectra of G, GO, and FGO; (**C**) TEM image of FGO; (**D**) UV absorption spectra of GO and FGO.

The morphologies of CdTe QDs were observed using TEM, which revealed simple, monodispersive, near-spherical shapes with a particle size distribution of 2–3 nm (Figure 2A,B). CdTe QDs exhibited narrow and sharp emission spectrum with a peak at 550 nm and emitted bright green fluorescence under excitation at 300 nm (Figure 2C). The transparent homogeneous solution of CdTe QDs was stable after 3 months, with no precipitation being evident. To confirm that CdTe-Apt had been successfully obtained, the

fluorescence spectra, FTIR spectra, and zeta potentials of CdTe QDs and CdTe-Apt QDs were measured. Due to the existence of phosphate groups in the aptamer, the spectrum of CdTe-Apt QDs exhibited a slight red shift; however, this had minimal impact on fluorescence characteristics (Figure 2D). These results were obtained with reference to our previous study [36]. CdTe QDs and CdTe-Apt had 3412 cm^{-1} O–H and 2864 cm^{-1} C–H stretching vibrations; this was judged to be responsible for the increase in carboxyl content on the synthesized CdTe-Apt surface (Figure 2E). In addition, the stretching vibration peaks of –NH, C–N, C=O, and N–C=O also appeared at 3065, 1654, 1568, and 1075 cm^{-1}, respectively, of CdTe-Apt, indicating that the $–NH_2$ of the aptamer reacted with the –COOH of the CdTe QDs. As can be seen from Figure 2F, the CdTe-Apt had a higher potential, further indicating that aptamer and CdTe QDs can be coupled through electrostatic interaction.

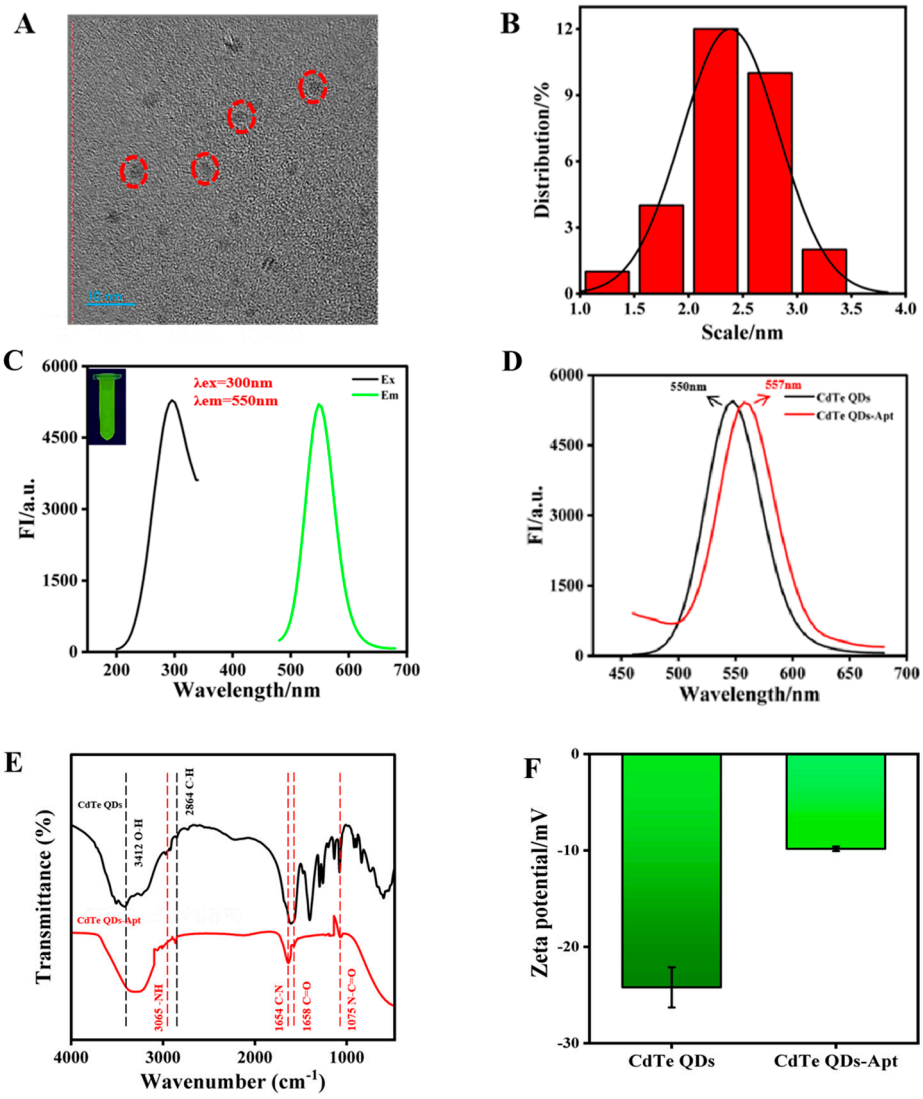


Figure 2. TEM image (**A**), particle size distribution (**B**), and fluorescence spectra (**C**) of CdTe QDs (illustration: fluorescence image); (**D**) fluorescence spectra of CdTe and CdTe-Apt QDs; (**E**) FT-IR spectra of CdTe and CdTe-Apt QDs; (**F**) zeta potentials of CdTe and CdTe-Apt QDs.

3.3. Feasibility Assessment of FGO/CdTe-Apt Aptasensor for AFB_1 Detection

The results of a feasibility assessment for the aptasensor detection of AFB_1 are shown in Figure 3. When there was no AFB_1 in the reaction system, the fluorescence signal of CdTe-Apt was as high as 3095 (a.u.) (green line). However, the addition of FGO significantly reduced its fluorescence intensity (black line) due to the π-π stacking interaction of

FGO with aptamer modified on CdTe QDs, which led to the formation of complexes in the ground state and also to the FRET effect, resulting in the lower fluorescence signal value measured by CdTe QDs fluorescence quenching. After the addition of AFB_1, the fluorescence value (red line) quickly increased to 2764 (a.u.), indicating that the AFB_1 aptamer could specifically bind to AFB_1, thus weakening the interaction between the aptamer and FGO, and recovering the fluorescence of CdTe QDs. Therefore, the fluorescence signal was high. The above results show that the aptasensor constructed for the present study can be used to successfully detect AFB_1.

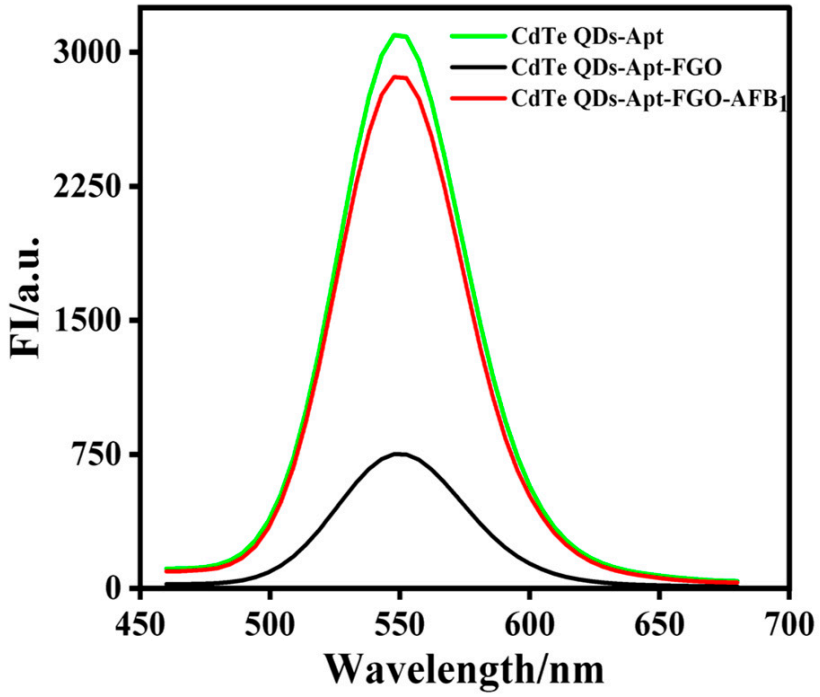


Figure 3. Feasibility of aptasensor for detecting AFB_1: fluorescence spectra of CdTe-Apt (green line), CdTe-Apt/FGO (black line), and CdTe-Apt/FGO + AFB_1 (red line).

3.4. Optimization Conditions of Aptasensing System

To obtain accurate detection results, relevant variables such as solution pH, incubation time, FGO concentration, and detection time were optimized. As can be seen in Figure 4A, CdTe-Apt fluorescence was affected by solution pH. Its fluorescence was relatively stable at pH values of 7–8 in the solution. The fluorescence attenuation of CdTe-Apt was attributed to the protonation of surface-bound carboxyl groups in acidic media or the protonation of hydroxide ions in alkaline media, leading to the destruction of the protective layer on the quantum dots [37]. PBS with pH 7.4 was selected because fluorescence attenuation of CdTe QDs was positively correlated with FGO content. As can be seen in Figure 4B, the fluorescence quenching ability of CdTe QDs was improved with FGO concentrations of up to 125 μg/mL. A 125 μg/mL concentration of FGO was therefore selected. To achieve the best FRET process, incubation times between FGO and CdTe-Apt were explored. CdTe-Apt fluorescence was almost completely quenched at 6 min (Figure 4C). After the addition of AFB_1, its fluorescence returned to the maximum value after 8 min. Hence, the detection time was determined to be 8 min.

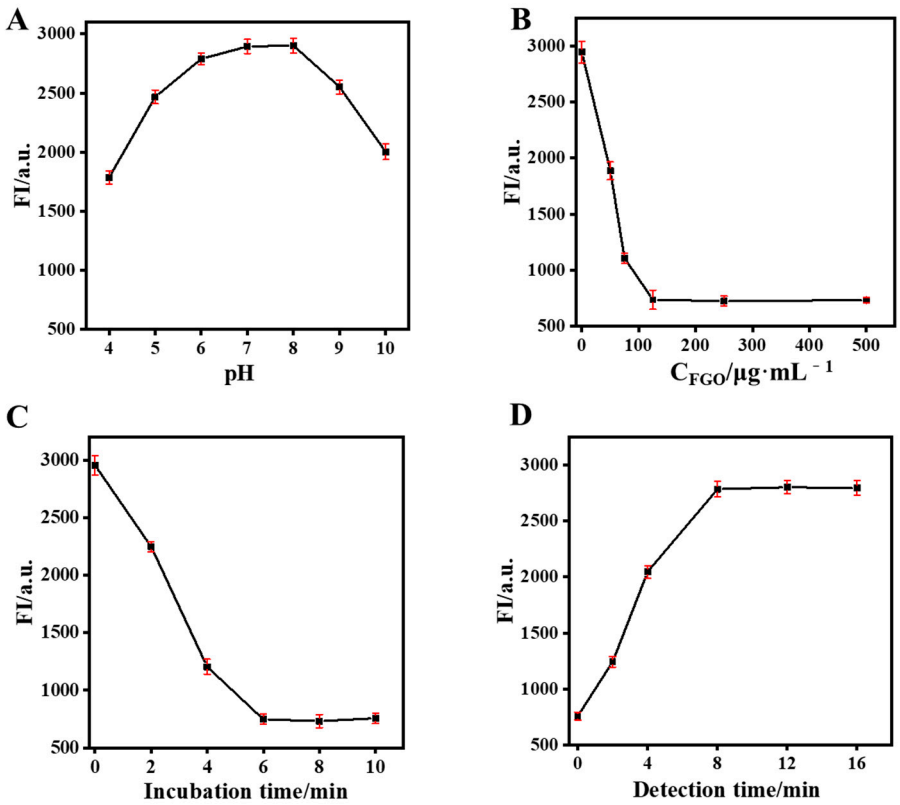


Figure 4. Effect of solution pH (**A**) and FGO concentration (**B**) on the fluorescence intensity of CdTe-Apt; effect of incubation (**C**) and detection (**D**) time on fluorescence intensity of CdTe-Apt/FGO and CdTe-Apt/FGO + AFB_1.

3.5. Performance of the Aptasensing System in AFB_1 Detection

The performance of the CdTe-Apt/FGO aptasensor in detecting AFB_1 was studied. In the optimal aptasensing system, the fluorescence intensity of CdTe-Apt returned to its highest value when the concentration of AFB_1 reached 150 ng/mL (Figure 5A,B). Values of ΔF (fluorescence response before and after the addition of AFB_1 into the aptasensor) and concentrations of AFB_1 in a range of 0.02–150 ng/mL exhibited a good linear relationship (Figure 5C). The equation was $y = 430.2 \log C_{AFB1} + 822.3$ with a regression coefficient (R^2) of 0.992, and the limit of detection (LOD) was 8.2 pg/mL. In addition, the green fluorescence of CdTe-Apt/FGO was observed to gradually increase under a UV lamp (Figure 5D). Table 1 summarizes recently reported methods for detecting AFB_1 based on aptasensors. The CdTe-Apt/FGO aptasensor was easy to obtain and operate, and it exhibited a great advantage with respect to LOD.

Table 1. Comparison of the aptasensor with methods used in previous studies for AFB_1 detection.

Mycotoxin	Method	Detection Range	LOD	Reference
AFB_1	UiO-66-NH_2/TAMRA/Apt	180 ng/mL	0.35 ng/mL	[38]
	QDs/AuNPs/Apt	10–400 nM	3.4 nM	[39]
	Ammonium Tetrastyrene/GO/Apt	0–3 ng/mL	0.25 ng/mL	[40]
	DNase/streptavidin magnetic beads/biotin/apt	0–200 ng/mL	22.6 ng/mL	[41]
	Si CDs/CdTe QDs/BHQ1/BHQ3/Apt	0.5–500 ng/mL	0.64 ng/mL	[42]
	CdTe-Apt/FGO	0.05–150 ng/mL	8.2 pg/mL	This work

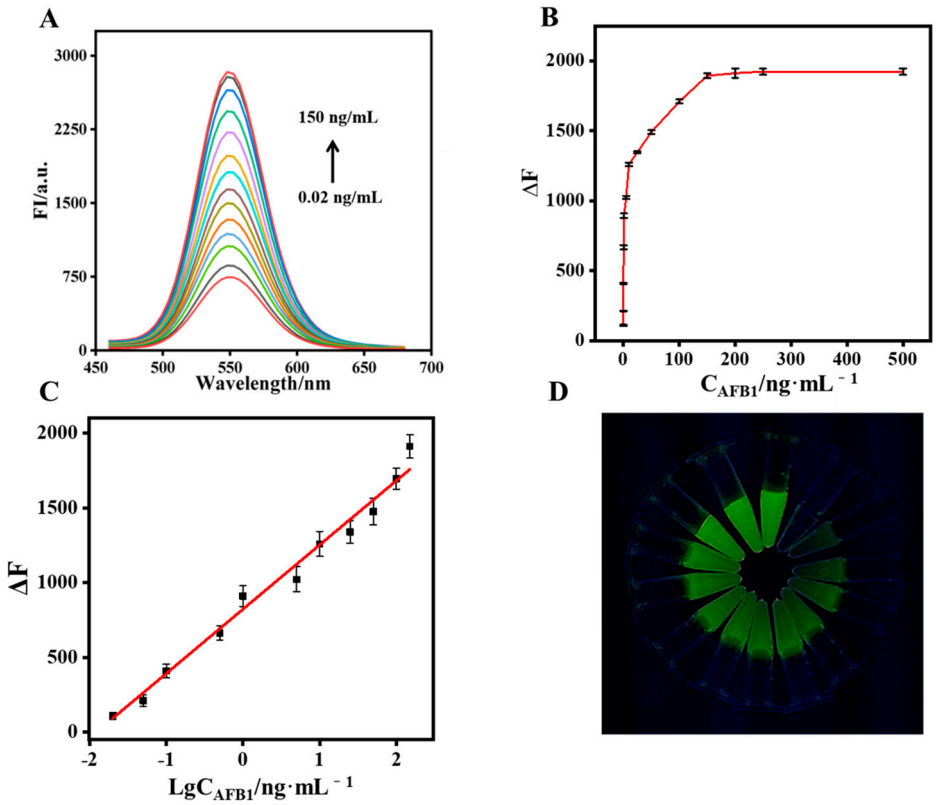


Figure 5. Fluorescence spectra (**A**) and fluorescence intensity (**B**) of the CdTe-Apt/FGO aptasensor for various concentrations of AFB_1; (**C**) relationship between ΔF and AFB_1 concentrations (0.02–150 ng/mL); (**D**) fluorescence changes in the Apt/FGO aptasensor under the UV lamp.

3.6. Selectivity and Stability of the Aptasensor

To verify the specificity of the aptasensor, fluorescence responses of CdTe-Apt/FGO in the presence of possible interferents, including AFM_1, FB_1, ZEN, DON, and PAT, were studied (Figure 6A). The selectivity of the aptasensor was evaluated by comparing the effects of different interfering substances on its fluorescence under the same detection conditions. The interferents barely affected the fluorescence of the aptasensor, even at concentrations five times higher than that of AFB_1. In addition, the fluorescence responses of the aptasensor were similar to those of AFB_1 alone and the mixed components of AFB_1 and interferents. This was due to the high affinity of the AFB_1 aptamer with AFB_1. The results indicated that the aptasensor had excellent selectivity for AFB_1 detection. The stability of the aptasensor was also evaluated. In Figure 6B, the aptasensor prepared in the same batch was stored at 4 °C and tested for AFB1 every 5 days. It can be seen that the aptasensor still responded well after 25 days of storage.

Pure milk and peanut powder were brought from a local supermarket for use as actual samples. The actual detection capability of the aptasensor was evaluated based on the standard addition method by adding AFB_1 into the treatment samples. The recovery rates of AFB_1 (0, 0.1, 1, and 10 ng/mL) after adding peanut or pure milk ranged from 94.5 to 107.0%, with the relative standard deviation (RSD) being less than 4.9%. These results were verified using HPLC standard methods (Table 2).

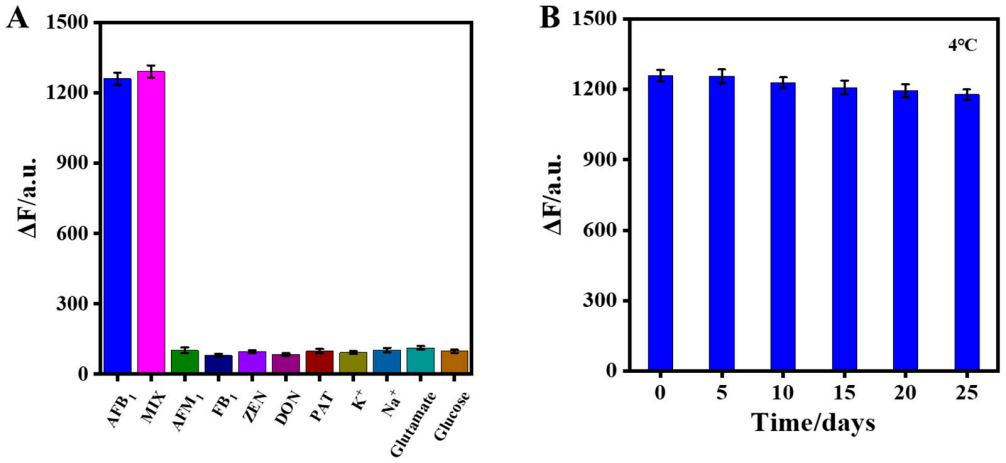


Figure 6. (**A**) Effect of the aptasensor on selectivity of AFB_1; (**B**) stability evaluation of the aptasensor at 4 °C over 25 days.

Table 2. Determination of AFB_1 in peanut and milk by aptasensor and HPLC (n = 3).

		Aptasensor			HPLC
	Added (ng/mL)	Found (ng/mL)	Recovery (%)	RSD (%, *n* = 3)	Found (ng/mL)
Peanut	0	-	-	-	-
	0.1	0.95 ± 0.03	94.5	4.9	-
	1	1.03 ± 0.11	103.4	2.7	1.02 ± 0.04
	10	9.76 ± 0.39	97.6	4.4	10.22 ± 0.12
Pure milk	0	-	-	-	-
	0.1	0.11 ± 0.04	107.0	4.7	-
	1	0.98 ± 0.16	98.1	1.7	1.03 ± 0.03
	10	10.48 ± 0.33	104.8	2.3	9.99 ± 0.11

4. Conclusions

In this study, a CdTe-Apt/FGO aptasensor was constructed for the purpose of AFB_1 detection. CdTe QDs modified with the AFB_1 aptamer (CdTe-Apt) were used as an energy donor, while FGO was used as an energy receptor. The π-π stacking interaction of FGO with CdTe-Apt led to the formation of complexes in the ground state. The CdTe-Apt strongly absorbed at the interface with the FGO layer, resulting in a FRET effect that quenched the fluorescence of CdTe QDs. Upon exposure to AFB_1, the aptamer modified on CdTe QDs formed a complex with the AFB_1; this weakened the adsorption between aptamer and FGO and assisted in restoring the fluorescence of CdTe QDs. This aptasensor exhibited a good linear range (0.02–150 ng/mL) and a low LOD (8.2 pg/mL) in detecting AFB_1. It also showed excellent selectivity and sensitivity in monitoring AFB_1 in pure milk and peanut samples, with recovery rates between 94.5% and 107.0%. In summary, the method introduced in the present study offers a new means of detecting AFB_1 in foods. The potential practical applications of this method are considerable; however, the potential impact on the environments and ecosystems of the release and degradation of quantum dots cannot be ignored. By enhancing research and development efforts, refining regulations, and elevating public awareness, we can effectively mitigate the potential risks associated with quantum dot technology, thereby bolstering its safe and efficient use in the rapid detection of food toxins.

Author Contributions: Conceptualization, X.H., T.W. and L.S.; methodology, P.L., S.L., K.Z. and L.S.; formal analysis, Q.H. and T.L.; investigation, Q.H. and X.H.; resources, K.Z., T.W. and L.S.; data

curation, P.L., S.L. and T.L.; writing—original draft preparation, P.L; writing—review and editing, T.W. All authors have read and agreed to the published version of the manuscript.

Funding: This work was supported by the National Natural Science Foundation of China (NO. 32101966) and the URCIP project of the School of Food Science and Technology, Henan Agricultural University.

Institutional Review Board Statement: Not applicable.

Informed Consent Statement: Not applicable.

Data Availability Statement: The data presented in this study are available on request from the corresponding author.

Conflicts of Interest: The authors declare no conflict of interest.

References

1. Cai, Q.; Zhu, L.; Chen, P. Effective Physical Methods for Aflatoxin B1 Removal in Food: A Comprehensive Review. *Food Control* **2025**, *173*, 111215. [CrossRef]
2. Damphathik, C.; Prakobkij, A.; Jarujamrus, P. Colorimetric sensor comprising metal-organic frameworks and molecularly imprinted polymers for aflatoxin B1 detection in agricultural commodities. *Food Chem.* **2025**, *474*, 143105. [CrossRef]
3. Ren, L.; Hong, F.; Wen, J. High-throughput colorimetry immunoassay for aflatoxin B1 detection using the synergistic regulation of click chemistry by polydopamine and metal-organic framework. *Food Chem.* **2025**, *475*, 143344. [CrossRef] [PubMed]
4. Eaton, D.L.; Williams, D.E.; Coulombe, R.A. Species differences in the biotransformation of aflatoxin B1: Primary determinants of relative carcinogenic potency in different animal species. *Toxins* **2025**, *17*, 30. [CrossRef] [PubMed]
5. Wang, R.; Zhang, Q.; Chen, G. Mechanistic insights into ferroptosis and apoptosis pathways: Synergistic effects of multi-organ toxicity and transgenerational effects induced by co-exposure of epoxiconazole and aflatoxin B1 in zebrafish. *J. Adv. Res.* 2025, *in press*. [CrossRef] [PubMed]
6. Zhao, L.; Yan, W.; Zhang, H. Antifungal and anti-aflatoxigenic mechanisms of dielectric barrier discharge cold plasma on Aspergillus flavus spores. *Innov. Food Sci. Emerg. Technol.* **2025**, *102*, 103964. [CrossRef]
7. Saini, S.S.; Abdel-Rehim, M. Integrated extraction approach for trace analysis of aflatoxin B1 in domestic water tanks using HPLC. *Sep. Sci. Plus* **2020**, *3*, 167–174. [CrossRef]
8. Teixeira, T.R.; Hoeltz, M.; Einloft, T.C. Determination of ochratoxin A in wine from the southern region of Brazil by thin layer chromatography with a charge-coupled detector. *Food Addit. Contam. Part B* **2011**, *4*, 289–293. [CrossRef]
9. Tonon, K.M.; Savi, G.D.; Scussel, V.M. Application of a LC–MS/MS method for multi-mycotoxin analysis in infant formula and milk-based products for young children commercialized in Southern Brazil. *J. Environ. Sci. Health Part B* **2018**, *53*, 685–691. [CrossRef]
10. Zhang, T.N.; Bai, W.J.; Zhao, K. Detection of aflatoxin B1 by a magnetic capture separator with time-resolved fluorescent microspheres. *Microchem. J.* **2024**, *199*, 110040. [CrossRef]
11. Han, S.; Yang, Y.; Chen, T. Quantitative Determination of Aflatoxin B1 in Maize and Feed by ELISA and Time-Resolved Fluorescent Immunoassay Based on Monoclonal Antibodies. *Foods* **2024**, *13*, 319. [CrossRef]
12. Hong, F.; Zhao, Y.; Pan, S. Click reaction-mediated fluorescent immunosensor based on Cu-MOF nanoparticles for ultrasensitive and high-throughput detection of aflatoxin B1 in food samples. *J. Agric. Food Chem.* **2024**, *72*, 5975–5982. [CrossRef]
13. Askari, A.; Kota, S.; Ferrell, H. UTexas Aptamer Database: The collection and long-term preservation of aptamer sequence information. *Nucleic Acids Res.* **2023**, *52*, 351–359. [CrossRef]
14. Yao, L.; Liu, T.; Sun, L. Selection of High-Affinity and Selectivity AFB1 Circular Aptamer for Biosensor Application. *J. Agric. Food Chem.* **2025**, *73*, 3222–3231. [CrossRef]
15. Sun, J.; Ning, X.; Cui, L. Sensitive detection of aflatoxin B1 in foods by aptasensing-based qPCR. *Food Chem.* **2024**, *432*, 137240. [CrossRef]
16. Quesada-González, D.; Merkoçi, A. Quantum dots for biosensing: Classification and applications. *Biosens. Bioelectron.* **2025**, *273*, 117180. [CrossRef]
17. Zhang, X.; Liu, C.; Liu, Z. Bioengineered two-dimensional nanomaterials (Bio-2DNMs) for cancer diagnosis and therapy: A comprehensive review. *Chem. Eng. J.* **2025**, *507*, 160430. [CrossRef]
18. Zheng, J.; Lian, Z.; Liu, T. A review for carbon dots-based fluorescent sensing tools for antibiotic and pesticide residues progress, challenge and perspective. *Food Control* **2025**, *172*, 111201. [CrossRef]
19. Zhang, H.; Yang, M.; Wu, Q. Engineering Two-Dimensional Nanomaterials for Photothermal Therapy. *Adv. Healthc. Mater.* **2024**, *64*, e202424768.

20. Mei, Y.; Cao, Y.; Wang, W. Emerging Violet Phosphorus Nanomaterial for Biomedical Applications. *Adv. Healthc. Mater.* **2015**, *14*, e2403576. [CrossRef]
21. Wang, T.; Zhang, K.; Jiang, M. Bone tumor diagnosis: A FRET-based fluorescent osteocalcin sensor using palladium nanoparticles. *Alex. Eng. J.* **2025**, *120*, 87–94. [CrossRef]
22. Chen, J.; Wu, H.; Zhang, W. Silica Coated Perovskite Quantum Dots with Single-Particle Level for Dual-Mode and Smartphone-Assisted Detection of Glutathione. *Sens. Actuators B* **2025**, *432*, 137489. [CrossRef]
23. Qin, Z.; Xu, J.; Cao, Y. Visual detection of glyphosate by Al^{3+}-regulated carbon dots/CdTe quantum dots ratiometric fluorescent sensing platform. *Food Chem.* **2025**, *473*, 143070. [CrossRef]
24. Kong, W.C.; Wu, X.H.; Li, C.C. A Label-Free Fluorescence Aptasensor for the Detection of Ciprofloxacin in Actual Samples. *ChemistrySelect* **2025**, *10*, e202405539. [CrossRef]
25. Lu, M.; Wang, T.; Li, T. Aptamer based ratiometric determination of DON by exploiting the FRET between carbon dots and graphene oxide. *J. Food Compos. Anal.* **2025**, *141*, 107384. [CrossRef]
26. Zeng, Z.; Li, W.; Zhang, J. Highly sensitive and specific graphene oxide-based FRET aptasensor for quantitative detection of human soluble growth stimulating gene protein 2. *Talanta* **2024**, *271*, 125629. [CrossRef]
27. Cai, Y.; Guo, G.; Fu, Y. A fluorescent aptasensor based on functional graphene oxide and FRET strategy simultaneously detects aflatoxins B1 and aflatoxins M1. *Chin. J. Anal. Chem.* **2024**, *52*, 100408. [CrossRef]
28. Chen, J.; Wang, C.; Huang, X. Quantum Dots-Engineered Flexible Hydrogel as Plant-Wearable Sensor for on-Site Profiling Dynamic Pesticide Degradation. *Adv. Funct. Mater.* **2025**, 2423643. [CrossRef]
29. Cui, W.; Hu, C.; Zhu, R. Low-background fluorescent biosensor based on graphene oxide and aptamer biorecognition for sensitive detection of kanamycin. *J. Food Compos. Anal.* **2024**, *131*, 106261. [CrossRef]
30. Fu, Z.; Chen, Z.; Yan, L. A RhB@ Tb-MOF sensor for selective detection of malachite green and leucomalachite green. *J. Food Compos. Anal.* **2025**, *140*, 107311. [CrossRef]
31. Xue, Y.; Bao, C.; Liu, H. BSA-Assisted Synthesis of Au Nanoclusters/MnO_2 Nanosheets for Fluorescence "Switch-On" Detection of Alkaline Phosphatase. *Biosensors* **2025**, *15*, 49. [CrossRef] [PubMed]
32. Goud, K.Y.; Hayat, A.; Satyanarayana, M. Aptamer-based zearalenone assay based on the use of a fluorescein label and a functional graphene oxide as a quencher. *Mikrochim. Acta* **2017**, *184*, 4401. [CrossRef]
33. Yoo, J.; Cho, Y.; Kim, D.H. Unraveling the role of Raman modes in evaluating the degree of reduction in graphene oxide via explainable artificial intelligence. *Nano Today* **2024**, *57*, 102366. [CrossRef]
34. Singh, G.; Devi, S.; Singh, A. Organosilane Functionalized Graphene Oxide Nanocomposite as Fluorescent Chemosensor for the Detection of Tyrosine in Aqueous Medium. *Appl. Organomet. Chem.* **2025**, *39*, e70081. [CrossRef]
35. Wang, B.; Liu, S.; Gao, M. A highly sensitive tapered fiber biosensor modified by PDMS combustion product and graphene oxide for MUC1 detection. *Sens. Actuators Rep.* **2025**, *9*, 100287. [CrossRef]
36. Liu, Z.; Zhou, J.; Wang, X. Graphene oxide mediated CdSe quantum dots fluorescent aptasensor for high sensitivity detection of fluoroquinolones. *Spectrochim. Acta Part A* **2024**, *305*, 123497. [CrossRef]
37. Yu, W.; Hao, A.; Mei, Y. A turn-on fluorescent aptasensor for ampicillin detection based on gold nanoparticles and CdTe QDs. *Microchem. J.* **2022**, *179*, 107454. [CrossRef]
38. Jia, Y.; Zhou, G.; Wang, X. A metal-organic framework/aptamer system as a fluorescent biosensor for determination of aflatoxin B1 in food samples. *Talanta* **2020**, *219*, 121342. [CrossRef]
39. Sabet, F.S.; Hosseini, M.; Khabbaz, H. FRET-based aptamer biosensor for selective and sensitive detection of aflatoxin B1 in peanut and rice. *Food Chem.* **2017**, *220*, 527–532. [CrossRef]
40. Jia, Y.; Wu, F.; Liu, P. A label-free fluorescent aptasensor for the detection of Aflatoxin B1 in food samples using AIEgens and graphene oxide. *Talanta* **2019**, *198*, 71–77. [CrossRef]
41. Setlem, K.; Mondal, B.; Shylaja, R. Dual Aptamer-DNAzyme based colorimetric assay for the detection of AFB1 from food and environmental samples. *Anal. Biochem.* **2020**, *608*, 113874.
42. Li, Y.; Sun, Q.; Chen, X. Simultaneous detection of AFB1 and aflD gene by "Y" shaped aptamer fluorescent biosensor based on double quantum dots. *Anal. Bioanal. Chem.* **2023**, *416*, 223–893.

Disclaimer/Publisher's Note: The statements, opinions and data contained in all publications are solely those of the individual author(s) and contributor(s) and not of MDPI and/or the editor(s). MDPI and/or the editor(s) disclaim responsibility for any injury to people or property resulting from any ideas, methods, instructions or products referred to in the content.